Journal of Asian Ceramic Societies 3 (2015) 144–150

HOSTED BY

Contents lists available at ScienceDirect

Journal of Asian Ceramic Societies

journal homepage: www.elsevier.com/locate/jascer

Fabrication of layered hydroxide zinc nitrate films and their conversion to ZnO nanosheet assemblies for use in dye-sensitized solar cells

Takuya Yuki[a], Shintaro Ueno[b], Manabu Hagiwara[a], Shinobu Fujihara[a,*]

[a] Department of Applied Chemistry, Faculty of Science and Technology, Keio University, 3-14-1 Hiyoshi, Kohoku-ku, Yokohama 223-8522, Japan
[b] Graduate School Department of Interdisciplinary Research, University of Yamanashi, 4-4-37 Takeda, Kofu 400-8510, Japan

ARTICLE INFO

Article history:
Received 26 August 2014
Received in revised form
18 December 2014
Accepted 27 December 2014
Available online 15 January 2015

Keywords:
Layered zinc hydroxide compound
Zinc oxide
Deposition
Microstructure
Dye-sensitized solar cells

ABSTRACT

Layered hydroxide zinc nitrate (LHZN; $Zn_5(NO_3)_2(OH)_8 \cdot xH_2O$) films were fabricated on glass or plastic substrates by a chemical bath deposition method combined with a homogeneous precipitation in methanolic solutions. High- or low-temperature pyrolytic decomposition of the LHZN films having two-dimensional morphology was attempted to obtain porous ZnO nanosheet-assembly films. The LHZN films were converted into porous ZnO films by pyrolyzing at temperatures above 400 °C, while porous LHZN/ZnO hybrid films were obtained by pyrolyzing at a lower temperature of 120 °C without morphological changes. The pyrolyzed ZnO films were applied to dye-sensitized solar cells (DSSCs), resulting in the generation of relatively high open-circuit voltages. The low-temperature pyrolysis enabled us to fabricate the LHZN/ZnO film even on the plastic substrate. Actually a cell using the LHZN/ZnO film on an indium tin oxide-coated polyethylene naphthalate substrate showed an energy conversion efficiency of 2.08% with a high open-circuit voltage around 0.70 V.

1. Introduction

Zinc oxide (ZnO) is a representative n-type metal-oxide semiconductor, which has a wide variety of optical and electrical applications. Generally the physical properties of ZnO depend largely on its microstructure. The morphological control of ZnO has therefore been intensively studied and various kinds of unique morphologies have been reported so far [1–4].

Pyrolytic decomposition is one of the effective approaches to control the morphology of metal oxides by changing/adjusting precursor materials. We have reported the microstructural control of porous ZnO films through the low-temperature pyrolysis of layered hydroxide zinc acetate (LHZA) films with flower-like [5], brussels sprouts-like [6], or nano-rectangular morphologies [7], layered hydroxide zinc carbonate (LHZC) films of a close nanosheet assembly [8], and layered hydroxide zinc benzoate (LHZB) films of a sparse nanosheet assembly [9]. One of the advantages of the pyrolytic decomposition of zinc-compound precursors is that architectures and/or crystallographic orientations of the precursors can be taken over by the resultant ZnO. Thus the microstructure of ZnO is not limited to that derived from its own crystal structure such as hexagonal plates [3], hexagonal prisms [4], and so on. In this study, we focus on layered hydroxide zinc nitrate (LHZN), in which nitrate ions are intercalated between zinc hydroxide layers, as a precursor for two-dimensionally (2D) microstructured ZnO films. Although there are many reports on the synthesis of LHZN powders by wet chemical processes [10,11], fabrication of LHZN films by a chemical solution method has seldom been reported so far except for a few reports on electrodeposited LHZN [12,13].

The application of the pyrolyzed layered zinc hydroxide films to ZnO electrodes in dye-sensitized solar cells (DSSCs) has remained a challenge. Nanoporous ZnO electrodes that were pyrolytically converted from the flower-like and the brussels sprouts-like LHZA films at 450 °C exhibited a light-to-electricity conversion efficiency of 4.6% and 5.1%, respectively [6]. Oriented ZnO films consisting of single-crystalline nanosheets with mesopores could be obtained by the pyrolysis of LHZC nanosheet-assembled films prepared by a homogeneous precipitation method [14,15]. The ZnO electrodes thus obtained showed a conversion efficiency over 5% due to a high specific surface area as well as an effective electron transport.

* Corresponding author. Tel.: +81 45 566 1581; fax: +81 45 566 1551.
E-mail address: shinobu@applc.keio.ac.jp (S. Fujihara).
Peer review under responsibility of The Ceramic Society of Japan and the Korean Ceramic Society.

http://dx.doi.org/10.1016/j.jascer.2014.12.006

In terms of a practical application of DSSCs, it has been attempted to replace transparent conductive oxide (TCO)-coated glass substrates with plastic substrates to fabricate flexible, lightweight, and cost-effective cells. For plastic substrates, porous metal-oxide semiconductors should be mounted below heat-proof temperatures of polymer materials used. We have already reported that dye-sensitized ZnO electrodes fabricated on indium tin oxide-coated polyethylene naphthalate (ITO-PEN) substrates by pyrolyzing LHZA films at 120 °C could give a relatively high conversion efficiency around 3.4% [16].

In the present work, we fabricated 2D microstructured LHZN films on ITO-PEN plastic as well as TCO glass substrates by combining a chemical bath deposition (CBD) and a homogeneous precipitation method. The LHZN films were then pyrolyzed at high or low temperatures. The resultant ZnO nanosheet-assembly films were applied to electrodes in DSSCs. Dependence of the DSSC performance on pyrolysis conditions was investigated to discuss the relationship between the film structure and cell parameters such as an open-circuit photovoltage (V_{OC}) and a short-circuit photocurrent density (J_{SC}).

2. Experimental

2.1. Fabrication of LHZN and ZnO films

LHZN films were fabricated by the CBD method combined with the homogeneous precipitation method using hexamethylenetetramine (HMT) as a precipitating agent. 75 mM $Zn(NO_3)_2{\cdot}6H_2O$ (99.0%, Wako Pure Chemical Industries Co. Ltd., Japan) and 250 mM HMT (99.0%, Wako) were dissolved in 10 mL of methanol, to which 1 mL of 2 M aqueous HNO_3 solution (60–61%, Taisei Kagaku Co. Ltd., Japan) was added. Borosilicate glass slides (S1111; Matsunami Glass Ind., Ltd., Japan) or fluorine-doped tin oxide-coated glass plates (FTO substrates; Nippon Sheet Glass Co. Ltd., Japan) were used as glass substrates, and ITO-PEN sheets (Touki Co. Ltd., Japan) were used as plastic substrates. They were immersed in the methanol solution and kept at a constant temperature of 60, 70, or 80 °C for 24 h. Films deposited on the glass substrates were rinsed with water and ethanol and dried at room temperature. Since the films were deposited on both sides of the substrates, the unnecessary film formed on the upper side was removed by scratching off. The resultant films were heated at temperatures between 400 and 500 °C for 0.5 h in a muffle furnace (designated a high-temperature pyrolysis method exclusively for the films on the glass substrates) or at 120 °C for the duration between 0.5 and 72 h in a drying oven (designated a low-temperature pyrolysis method).

2.2. Characterization

Crystal structures of the films obtained were identified by an X-ray diffraction analysis (XRD; D8-02 diffractometer, Bruker AXS) using CuKα radiation. The microstructure of the films was observed by a scanning electron microscope (SEM; Inspect S50, FEI) and a field-emission transmission electron microscope (FE-TEM; TECNAI F20, Philips). Thermal behavior of the LHZN films was examined by thermogravimetry-differential thermal analysis (TG-DTA; DTG-60, Shimadzu). The pH value of the solutions was measured by a pH meter (F-51, Horiba). Functional groups of chemical species of the films were analyzed by Fourier transform infrared spectroscopy (FT-IR; ALPHA, Bruker) using a KBr pellet method. A Brunauer–Emmett–Teller (BET) specific surface area was evaluated by a nitrogen gas adsorption/desorption method using an automatic surface area and porosimetry analyzer (Tristar 3000, Shimadzu).

2.3. DSSC measurement

The ZnO films obtained on the FTO glass or the ITO-PEN plastic substrates were immersed in a 0.3 mM $RuL_2(NCS)_2$:2TBA (L = 2,2′-bipyridyl-4,4′-dicarboxylic acid and TBA = tetrabutylammonium; N719, Solaronix SA, Switzerland) ethanolic solution at 60 °C for 0.5 h. Sandwich-type open cells were constructed with the ZnO/N719 electrode, a spacer film (50 μm in thickness), and a counter platinum electrode. An I^-/I_3^- redox couple electrolyte, which was composed of 0.1 M LiI (97.0%, Wako), 50 mM I_2 (99.8%, Kanto Chemical Co. Inc., Japan), 0.6 M 1,2-dimethyl-3-propylimidazolium iodide (DMPII; Shikoku Chemicals Corp., Japan), 1.0 M 4-tert-butylpyridine (96%, Sigma–Aldrich Co. LLC, USA), and 3-methoxypropionitrile (99.0%, Wako), was introduced between the electrodes. An active cell area was fixed at 25 mm^2 by a mask.

The cell parameters, V_{OC}, J_{SC}, a fill factor (*ff*), and the conversion efficiency (η), were determined by *J*–*V* measurements (*J*: photocurrent density, *V*: photovoltage). A 500 W Xenon lamp (UXL-500SX, Ushio) was used as a light source to produce the simulated AM 1.5 illumination at 100 mW cm^{-2}. An AM 1.5 filter, a water filter, and an infrared cut filter (S76-HA50, Hoya) were placed in the light path to regulate the light in a wavelength range of 300–800 nm, reducing a mismatch of the simulated sunlight. *J*–*V* curves were measured with a potentiostat (HSV-100, Hokuto Denko) under the simulated sunlight. Dark current–voltage curves were also measured in the same way under a dark condition.

The amount of dyes adsorbed on the ZnO electrodes was estimated by measuring the absorbance of desorbed dyes. Desorption was carried out by immersing in a 0.5 M NaOH ethanol/water (v/v = 1) solution. Absorbance of the resultant dye solutions was measured by a spectrophotometer (V-670, Jasco) and calibrated with a standard solution of N719.

3. Results and discussion

3.1. Characterization of LHZN films

Fig. 1(a) shows XRD patterns of the films deposited at 60, 70, or 80 °C for 24 h on the glass slides. The films deposited at the higher temperatures (70 or 80 °C) are identified as a wurtzite-type ZnO. In contrast, a pattern of the film deposited at 60 °C is similar to those of layered zinc hydroxide nitrates, $Zn_5(NO_3)_2(OH)_8$ (ICDD 25-1028) and $Zn_5(NO_3)_2(OH)_8{\cdot}2H_2O$ (ICDD 24-1460). A diffraction peak at $2\theta = 9.59°$ ($d = 9.23$ Å, corresponding to a basal spacing of layered compounds) is located between that of $Zn_5(NO_3)_2(OH)_8$ ($d = 8.98$ Å) and $Zn_5(NO_3)_2(OH)_8{\cdot}2H_2O$ ($d = 9.79$ Å). Generally, a basal spacing of the layered zinc hydroxide compounds varies with compositions of intercalated anion species and/or water molecules [17,18]. A content of intercalated water molecules in the present LHZN may be smaller than that of $Zn_5(NO_3)_2(OH)_8{\cdot}2H_2O$, which was synthesized in an aqueous solution, because it was obtained from the methanol solution mixed only with the very small amount of the aqueous HNO_3 solution.

Fig. 1(b) shows SEM images of the surface of the films deposited at 60, 70, or 80 °C for 24 h on the glass slides. Hexagonal prismatic particles of ZnO are precipitated on the glass at 70 or 80 °C. ZnO is assumed to be produced preferentially at the higher temperatures because an OH^- concentration of the solution increases drastically by a temperature-promoted thermohydrolysis of HMT expressed by following equations [19]:

$$(CH_2)_6N_4 + 6H_2O \rightarrow 6HCHO + 4NH_3 \quad (1)$$

$$NH_3 + H_2O \rightarrow NH_4^+ + OH^- \quad (2)$$

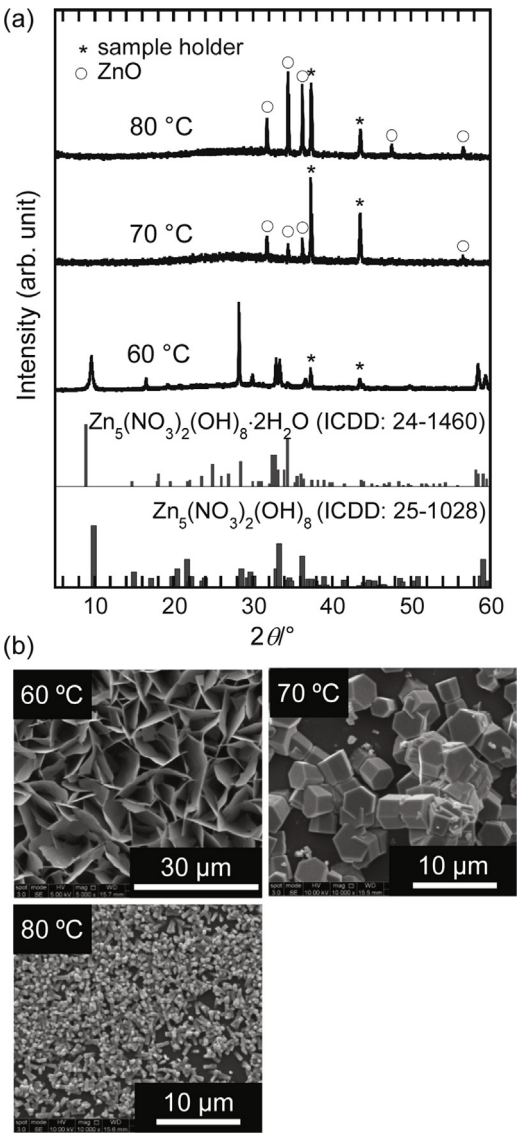

Fig. 1. (a) XRD patterns and (b) SEM images of the films deposited on the glass slides at 60, 70, or 80 °C for 24 h.

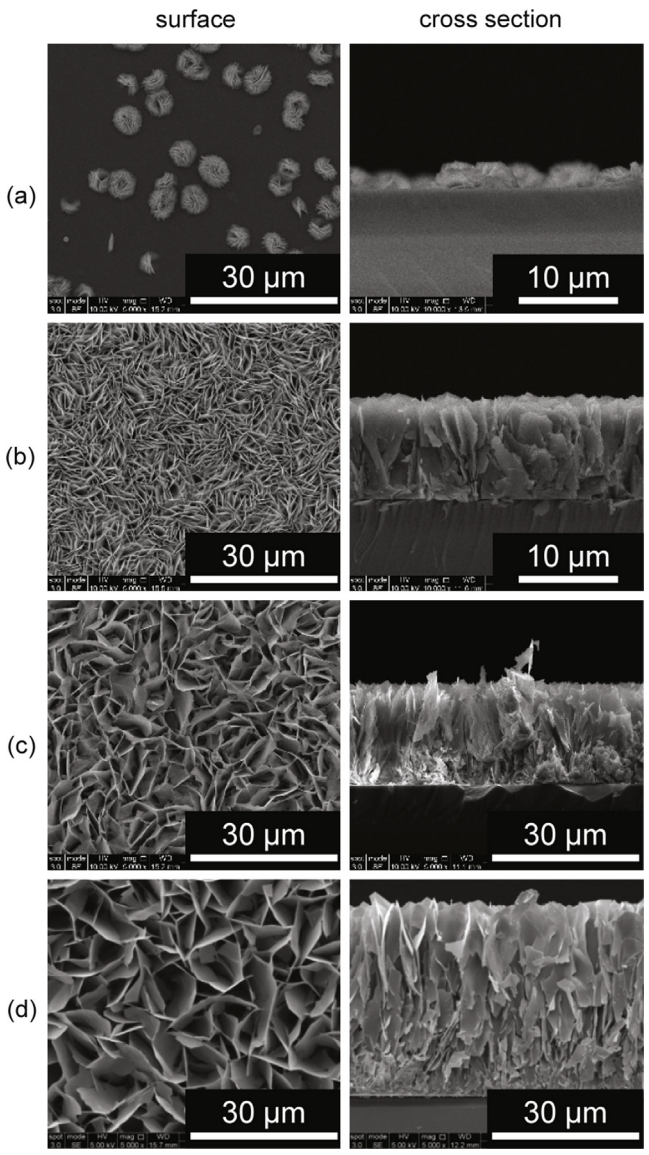

Fig. 2. Surface and cross-section SEM images of the LHZN films deposited on the glass slides at 60 °C for (a) 3, (b) 6, (c) 12, or (d) 24 h.

Under the strongly basic condition, the oxolation of Zn^{2+} ions to form metaloxane networks is dominant over the olation [20]. As seen in Fig. 1(b), the particle size of ZnO is decreased considerably with increasing the temperature, suggesting that the nucleation rate of ZnO is increased at the higher temperature and simultaneously the growth of the individual ZnO particles is suppressed. In contrast, the olation of Zn^{2+} ions leads to the formation of positively charged zinc hydroxide layers under the weakly basic condition, and then LHZN crystals are formed with the intercalation of NO_3^- anions between the layers. As also seen in Fig. 1(b), upstanding LHZN nanosheets grow on the glass to form 2D microstructured film at 60 °C.

The layered zinc hydroxide compounds commonly prefer 2D microstructures such as nanosheets and nanoplates, resulting from a difference in the growth rate of each plane in the anisotropic crystal structure. In the case of LHZN, the growth rate along the *a*-axis (perpendicular to the zinc hydroxide basal planes) is much slower than that along the *b*- and *c*-axes (parallel to the zinc hydroxide basal planes) [10]. To investigate a growth mechanism of the LHZN nanosheet assembly, the progress of the deposition at 60 °C between 0.5 and 24 h was monitored by measuring the pH value of the solution and observing the microstructure of the films. Note that all the deposited films were preliminarily identified as LHZN by the XRD analysis. The pH value of the solution increased from 4.8 to 5.5 at the initial stage of the reaction (0.5 h). The OH^- ions were continuously supplied by the thermohydrolysis of HMT (Eqs. (1) and (2)) and consumed by the following LHZN formation reaction:

$$5Zn^{2+} + 2NO_3^- + 8OH^- + xH_2O \rightarrow Zn_5(NO_3)_2(OH)_8{\cdot}xH_2O \quad (3)$$

Actually the pH value was almost unchanged after 24 h (pH 5.6).

Fig. 2 shows the microstructure of the films deposited at 60 °C for the duration between 3 and 24 h. In Fig. 2(a), it is seen that the substrate is covered in spots with the LHZN nanosheets which were radially grown. This indicates the progress of the heterogeneous nucleation of LHZN at the early stage of the reaction within 3 h. Such hemispheric assemblies of nanosheets were also seen in the other layered zinc oxides such as LHZA and LHZB in the early stage of the film formation [9,18]. Thus, the growth mechanism of the LHZN film can be explained following that of the other layered zinc hydroxide compounds [18]. Thin LHZN plates grow with its (1 0 0) plane parallel to the substrate at the initial stage of the film formation. The plates are then branched gradually with the progress

of the crystal growth. The growth direction of the LHZN films is bent toward the bulk of the solution due to the concentration gradient formed near the LHZN plates, resulting in the formation of the hemispheric assemblies. With increasing the deposition time to 6 h, the substrate is covered with the LHZN film and the growth direction is changed to the direction perpendicular to the substrate surface (Fig. 2(b)). Interspaces between the nanosheets are being expanded and hence the film density is decreased with the deposition time up to 24 h (Fig. 2(c) and (d)). It may result from a decrease in the concentration of the reactants in Eq. (3). The film thickness observed in cross section images in Fig. 2 increases monotonically with the deposition time and reaches approximately 40 μm after 24 h.

In the following, we used the LHZN films deposited at 60 °C for 24 h because of their 2D microstructure suitable for DSSCs. For this purpose, the LHZN films were deposited also on the FTO and the ITO-PEN substrates. The thickness of the films fell in the range of 17–33 μm, which was enough for the application to DSSCs.

3.2. High-temperature pyrolytic conversion from LHZN to ZnO

The LHZN films deposited on the glass slides were heat-treated at 400, 450, or 500 °C for 0.5 h. As shown in Fig. 3(a), XRD patterns of the resultant films are assigned to ZnO irrespective of the heating temperature. Fig. 3(b) shows SEM images of the surface of the ZnO films thus obtained. Any of the films maintains the sheet-like architecture of the original LHZA. However, the respective nanosheets seem to be changed to gathered small particles and their porosity increases with increasing the pyrolyzing temperature. This can be explained by the temperature-promoted grain growth of ZnO and a similar tendency is seen in the other pyrolyzed layered zinc hydroxide compounds [6].

The ZnO nanosheet-assembled films were fabricated on the FTO substrates by the high-temperature pyrolysis to be applied as electrodes in DSSCs. *J–V* curves and dark current–voltage curves of the cells using the ZnO films pyrolyzed at 400, 450, or 500 °C are shown in Fig. 4. Cell parameters determined from the *J–V* measurement are summarized in Table 1. A higher V_{OC} of 0.760 V is obtained for the cell with the ZnO electrode pyrolyzed at 500 °C. Generally the high-temperature pyrolysis results in a smaller specific surface area of the electrode, which corresponds to an effective decrease in surface defects working as recombination sites to improve V_{OC} [21]. Actually, the magnitude of the dark current of this cell is much smaller than those of the other cells at the same applied voltage above 0.50 V (near the flat-band potential of the ZnO electrode), indicative of the suppressed recombination. Due to a smaller J_{SC} (3.75 mA cm^{-2}), however, a conversion efficiency is lower with the electrode pyrolyzed at 500 °C.

The ZnO electrodes pyrolyzed at 400 or 450 °C show the comparable V_{OC} of approximately 0.71 V. J_{SC} of the electrode pyrolyzed at 450 °C is larger than that at 400 °C in spite of the similar amount of the adsorbed dyes. The photocurrent in DSSCs is related not only to a light-harvest efficiency but also to an electron injection efficiency and an electron collection efficiency [22,23]. The electrode pyrolyzed at 400 °C may have a poor connection among the ZnO particles due to a lower degree of sintering, leading to a lower electron collection efficiency. The fill factor of the electrode pyrolyzed at 400 °C is much smaller than that of the electrode at 450 °C, also suggesting the lower electrical conduction (the higher resistance) of the electrode heated at the lower temperature. It is curious that the electrode pyrolyzed at 500 °C also has the smaller fill factor than the electrode at 450 °C, contrary to the higher V_{OC}. This might result from the degraded contact between the ZnO film and the FTO substrate due to the larger shrinkage of the film during heating. The degradation of the electrical contact would increase the resistance at the ZnO/FTO interface, thus leading to the decrease in the fill factor. A similar tendency was also found in our previous report; the fill factor of the ZnO electrodes prepared by pyrolyzing the LHZA films on the FTO substrate at temperatures of 600 °C or higher was smaller than that of the ZnO electrodes pyrolyzed at 400–550 °C [21].

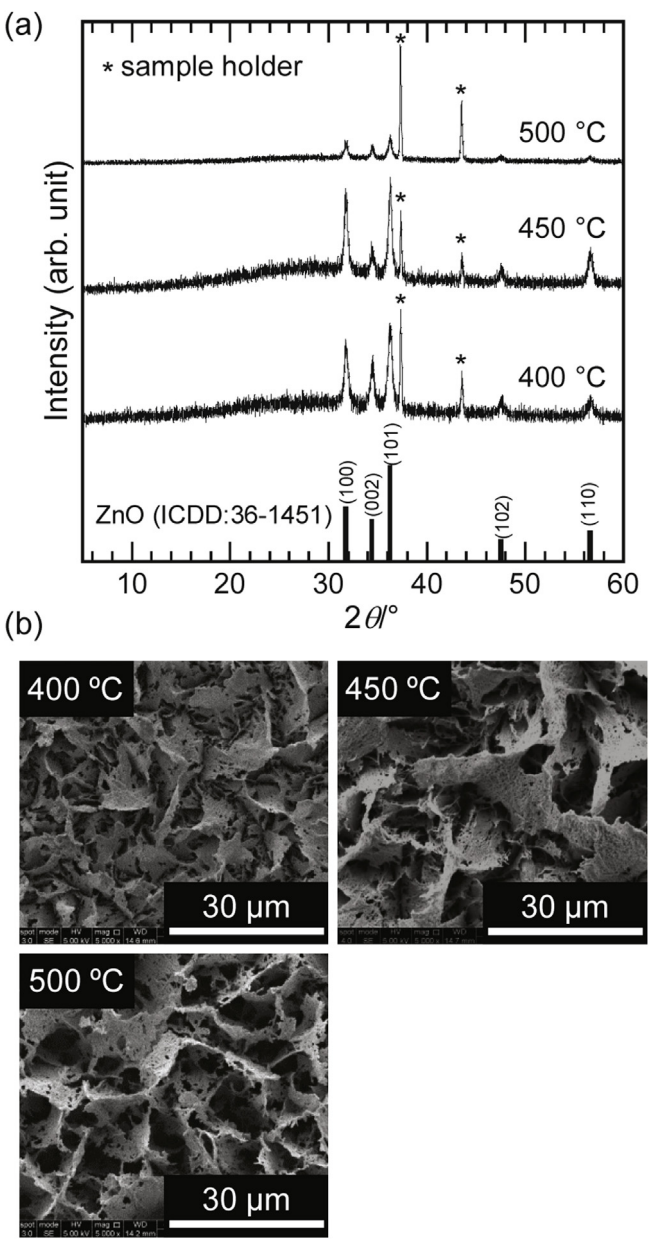

Fig. 3. (a) XRD patterns and (b) SEM images of the films obtained by pyrolyzing the LHZN films on the glass slides at 400, 450, or 500 °C for 0.5 h.

In summary of the high-temperature pyrolytic conversion, the highest conversion efficiency of approximately 3.0% was obtained for the LHZN-derived ZnO electrode pyrolyzed at 450 °C in the present study.

3.3. Low-temperature pyrolytic conversion from LHZN to ZnO

Fig. 5 shows XRD patterns of the films on the glass slides after pyrolyzing at 120 °C for various durations. Diffraction peaks due to ZnO appear after 6 h. The conversion from LHZN to ZnO is further promoted with increasing the duration. However, the conversion is not completed even after 72 h. Details of the pyrolytic conversion were then analyzed with TG-DTA, following a similar examination

Table 1
Characteristic values of the cells using the ZnO electrodes obtained by pyrolyzing the LHZN films on the FTO substrates at 400, 450, or 500 °C for 0.5 h.

Pyrolyzing temperature (°C)	V_{OC} (V)	J_{SC} (mA cm^{-2})	ff (–)	η (%)	Dye adsorption (10^{-8} mol cm^{-2})
400	0.709	4.54	0.439	1.41	4.47
450	0.707	6.53	0.652	3.01	4.67
500	0.760	3.75	0.524	1.49	3.63

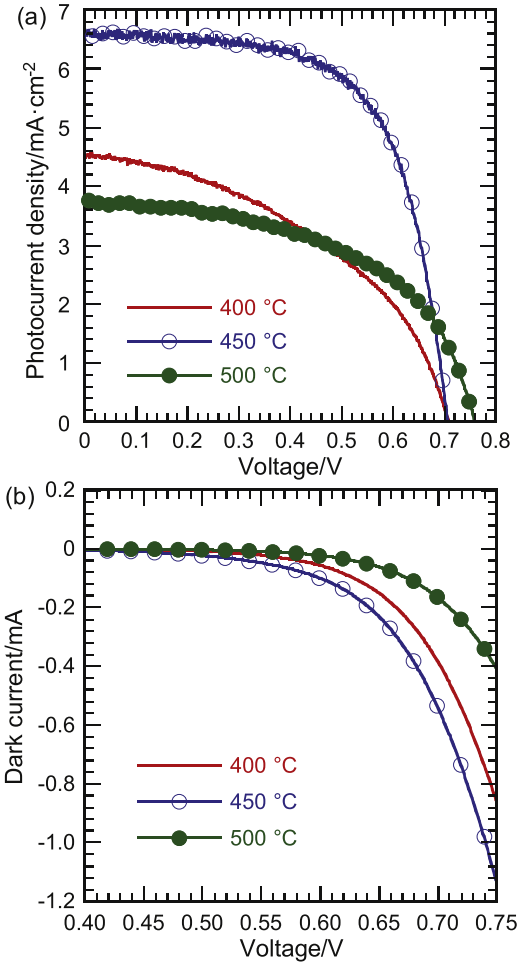

Fig. 4. (a) *J–V* curves and (b) dark current–voltage curves of the cells using the ZnO electrodes obtained by pyrolyzing the LHZN films on the FTO substrates at 400, 450, or 500 °C for 0.5 h.

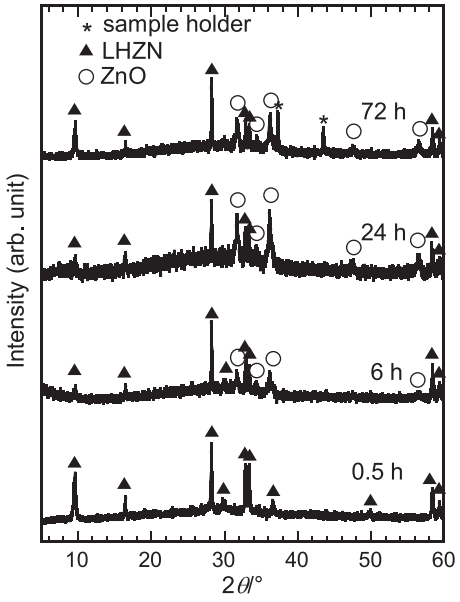

Fig. 5. XRD patterns of the films obtained by pyrolyzing the LHZN films on the glass slides at 120 °C for 0.5, 6, 24, or 72 h.

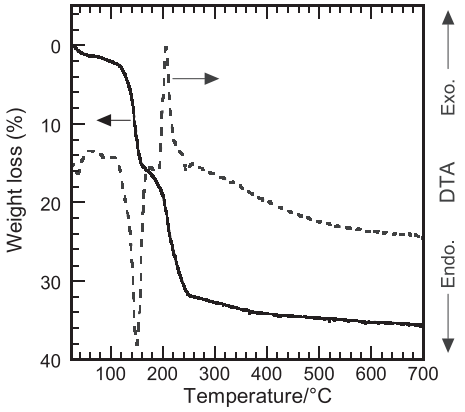

Fig. 6. TG-DTA curves of the LHZN sample obtained at 60 °C for 24 h.

reported in the literature. The pyrolysis of $Zn_5(NO_3)_2(OH)_8{\cdot}2H_2O$ can be divided into three stages, and the first and the second stage are expressed as follows [12,24–26]:

$$Zn_5(NO_3)_2(OH)_8{\cdot}2H_2O \rightarrow Zn_5(NO_3)_2(OH)_8 + 2H_2O \quad (65\text{–}110\,^{\circ}C) \tag{4}$$

$$Zn_5(NO_3)_2(OH)_8 \rightarrow Zn_3(NO_3)_2(OH)_4 + 2ZnO + 2H_2O \quad (120\text{–}150\,^{\circ}C) \tag{5}$$

At the first stage, the intercalated water molecules are removed at temperatures up to 110 °C. Then, the dehydrated $Zn_5(NO_3)_2(OH)_8$ is partially decomposed to $Zn_3(NO_3)_2(OH)_4$ and ZnO at temperatures between 120 and 150 °C. At the third stage, the pyrolysis of the resultant $Zn_3(NO_3)_2(OH)_4$ proceeds in any of two possible reaction pathways [12,24,26]:

$$Zn_3(NO_3)_2(OH)_4 \rightarrow 3ZnO + 2HNO_3 + H_2O \quad (140\text{–}170\,^{\circ}C) \tag{6}$$

$$4Zn_3(NO_3)_2(OH)_4 \rightarrow 9ZnO + 3Zn(NO_3)_2 + 2HNO_3 + 7H_2O \quad (150\text{–}205\,^{\circ}C) \tag{7-1}$$

$$Zn(NO_3)_2 \rightarrow ZnO + NO_2 + NO + O_2 \quad (205\text{–}250\,^{\circ}C) \tag{7-2}$$

When the intermediate $Zn(NO_3)_2$ is once formed, the overall pyrolysis process needs higher temperatures. A theoretical weight loss associated with the conversion from $Zn_5(NO_3)_2(OH)_8{\cdot}2H_2O$ to ZnO is calculated to be 34.7%.

Fig. 6 shows TG-DTA curves of the LHZN film deposited at 60 °C for 24 h. A weight loss of 1.4% at temperatures up to 60 °C with a minor endothermic peak around 40 °C is attributed to the removal of physically adsorbed methanol molecules. A next weight loss of

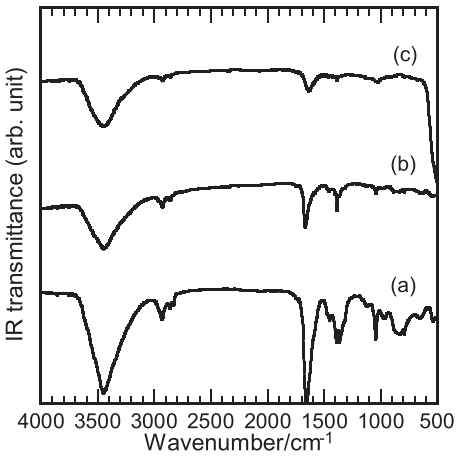

Fig. 7. FT-IR spectra of (a) the as-prepared LHZN film and the films pyrolyzed (b) at 120 °C for 72 h or (c) at 450 °C for 0.5 h.

2.3% up to 110 °C is smaller than a theoretical weight loss of 5.8% calculated with Eq. (4), suggesting a different water content between the present LHZN and the reported $Zn_5(NO_3)_2(OH)_8{\cdot}2H_2O$. Weight losses of 13.5% with an endothermic peak and 16.1% with an exothermic peak are observed in the temperature range of 100–160 and 160–250 °C, respectively. Such weight losses do not correspond to theoretical ones for the respective reaction steps (Eqs. (5), (6), or (7-1)). These reactions may proceed in parallel, judging from the fact that a total weight loss is 29.6%, which is close to a theoretical loss of 28.9% for the conversion from $Zn_5(NO_3)_2(OH)_8$ to ZnO. In addition, the net weight loss of the present LHZN after releasing the physically adsorbed species is 30.5%. This is smaller than a theoretical weight loss of 34.7% from $Zn_5(NO_3)_2(OH)_8{\cdot}2H_2O$, which may be related to the compositional difference in the intercalated water as found in the XRD analysis (Fig. 1(a)).

The TG-DTA results suggest that the condensation of the zinc hydroxide layers and the release of the nitrate ions can take place simultaneously, following the respective reaction pathways (Eqs. (6) or (7-1,2)). In fact, the LHZN film was not pyrolyzed completely and hence the LHZN/ZnO hybrid film was obtained by the low-temperature pyrolysis method. Fig. 7 compares FT-IR spectra of the as-prepared LHZN film and the films pyrolyzed at 120 °C for 72 h or at 450 °C for 0.5 h. Strong absorption bands are observed at around 3450 and 1640 cm^{-1} in all the samples, resulting from stretching and bending modes, respectively, of intercalated or physically adsorbed H_2O. For the as-prepared LHZN film and the pyrolyzed film at 120 °C, absorption bands centered at around 1385, 1040, and 830 cm^{-1} clearly indicate the presence of the nitrate ions. Additionally, absorption bands appearing between 3000 and 2800 cm^{-1} may suggest the presence of undecomposed HMT and/or physically adsorbed methanol inside the films. Small absorption bands centered at around 640 cm^{-1}, which are ascribed to the δ mode of O—H groups in the hydroxide layers, are also found for the as-prepared LHZN film and the pyrolyzed film at 120 °C [12,25]. In contrast, the above-mentioned bands are hardly found in the ZnO film heated at 450 °C for 0.5 h, indicative of the complete pyrolysis.

Fig. 8 shows SEM images of the film obtained by pyrolyzing the LHZN film at 120 °C for 72 h. The morphology and the thickness of the film obtained by the low-temperature pyrolysis are almost the same as those of the initial LHZN film. In contrast to the porous ZnO films obtained by the high-temperature pyrolysis shown in Fig. 3(b), the surface of the nanosheets in Fig. 8 seems to be smooth at a low magnification.

Fig. 9 compares TEM images of the LHZN films pyrolyzed at 450 °C for 0.5 h or at 120 °C for 72 h. Lager nanoparticles

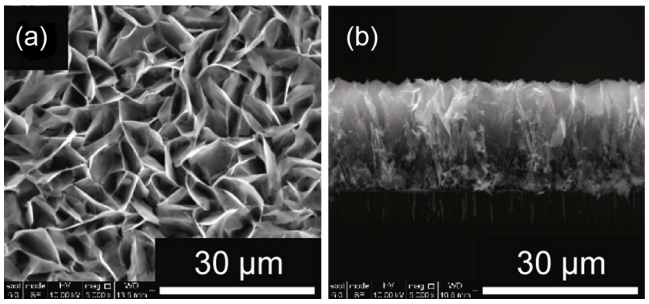

Fig. 8. (a) Surface and (b) cross-section SEM images of the film obtained by pyrolyzing the LHZN film on the glass slide at 120 °C for 72 h.

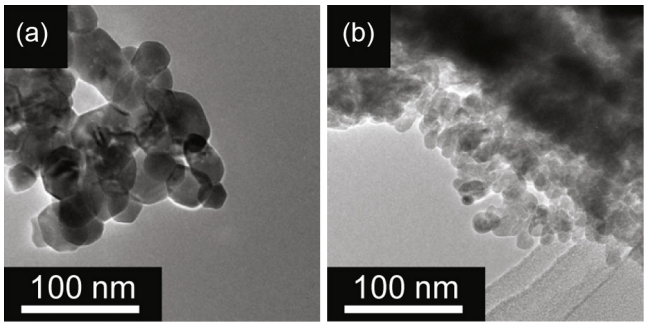

Fig. 9. FE-TEM images of the films obtained by pyrolyzing the LHZN films on the glass slides (a) at 450 °C for 0.5 h or (b) at 120 °C for 72 h.

approximately 40 nm in size are obtained in the ZnO film pyrolyzed at 450 °C (Fig. 9(a)), as a result of the grain growth. At the low pyrolysis temperature of 120 °C, smaller nanoparticles approximately 20 nm in size are observed in the LHZN/ZnO film. It was confirmed that these nanoparticles were ZnO by measuring the spacing of lattice fringes. The relatively smooth surface observed in the SEM image for the LHZN/ZnO film is related to the smaller particle size as well as the hybrid nature.

The BET specific surface area of the pyrolyzed films was evaluated by the nitrogen gas adsorption/desorption method. The LHZN/ZnO film through the low-temperature pyrolysis had a slightly higher specific surface area of 18.9 $m^2\,g^{-1}$ than that of 13.1 $m^2\,g^{-1}$ for the ZnO film through the high-temperature pyrolysis.

The performance of DSSCs using the LHZN/ZnO hybrid films fabricated on the FTO or the ITO-PEN substrate by the low-temperature pyrolysis method at 120 °C for 72 h is summarized in Table 2. The amount of adsorbed dyes in these hybrid electrodes is larger than that in the ZnO electrodes through the high-temperature pyrolysis (see Table 1) because of the different specific surface areas. Fig. 10 compares *J*–*V* curves and dark current–voltage curves of the cells using the electrodes obtained by pyrolyzing the LHZN films at 450 °C for 0.5 h or at 120 °C for 72 h on the FTO or the ITO-PEN substrate. In spite of the relatively large amount of adsorbed dyes, the photocurrent density (including J_{SC}) of the LHZN/ZnO electrodes through the low-temperature pyrolysis is smaller than that of the ZnO electrode through the high-temperature pyrolysis. The dark current of the LHZN/ZnO electrodes is also much smaller even at higher applied voltages. These facts imply that the effective electron transport to generate the current is limited to a region near the ZnO/FTO interface in the LHZN/ZnO electrodes with the higher resistance. That is, the electrons injected from dyes only near the ZnO/FTO interface contribute to the current generation. Under this situation, neither the high resistance nor the recombination would influence largely the V_{OC} and the *ff* values. Actually, the LHZN/ZnO electrodes are comparable to the ZnO electrodes

Table 2
Characteristic values of the cells using the ZnO electrodes on the FTO or the ITO-PEN substrate obtained by the low-temperature pyrolysis method (at 120 °C for 72 h).

Substrate	V_{OC} (V)	J_{SC} (mA cm^{-2})	*ff* (–)	η (%)	Dye adsorption (10^{-8} mol cm^{-2})
FTO	0.673	4.18	0.714	2.01	7.16
ITO-PEN	0.696	4.70	0.635	2.08	7.32

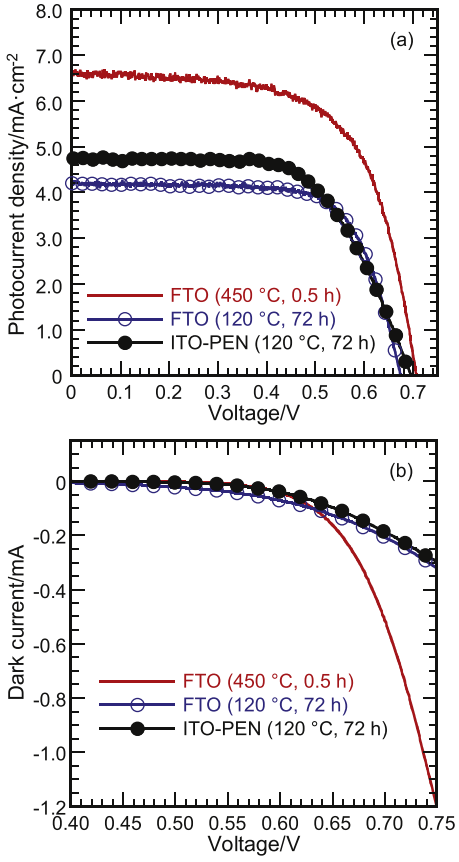

Fig. 10. (a) *J*–*V* curves and (b) dark current–voltage curves of the cells using the ZnO electrodes obtained by pyrolyzing the LHZN films on the FTO substrates at 450 °C for 0.5 h or at 120 °C for 72 h and the LHZN film on the ITO-PEN substrate at 120 °C for 72 h.

through the high-temperature pyrolysis in terms of V_{OC} and *ff*, leading to the conversion efficiency more than 2%. Such a result is promising for a further improvement of the low-temperature processed electrode if the problem of the electrical conduction is overcome with a microstructural control through, for example, a dissolution–reprecipitation cycle in liquid media [27].

4. Conclusions

The LHZN nanosheet-assembly films were fabricated on the glass or the plastic substrates by the CBD method combined with the homogeneous precipitation method using HMT as the precipitating agent in the methanolic solutions. The LHZN films were pyrolytically converted into the ZnO and the LHZN/ZnO hybrid films without morphological changes by the high- and the low-temperature pyrolysis method, respectively. The pyrolysis temperature influenced the size of the ZnO crystallites constituting the pyrolyzed films and correspondingly the amount of adsorbed dyes in application to the DSSC electrodes. Generally the cells using the present ZnO or the LHZN/ZnO electrodes exhibited the relatively high V_{OC} values. Accordingly the LHZN/ZnO hybrid electrode on the ITO-PEN substrate showed the energy conversion efficiency of 2.08% with V_{OC} around 0.70 V. Our method is then promising for the facile fabrication of plastic DSSCs.

References

[1] Y.J. Lee, T.L. Sounart, J. Liu, E.D. Spoerke, B.B. McKenzie, J.W.P. Hsu and J.A. Voigt, Cryst. Growth Des., 8, 2036–2040 (2008).
[2] M. Law, L.E. Greene, J.C. Johnson, R. Saykally and P. Yang, Nat. Mater., 4, 455–459 (2005).
[3] L.P. Bauermann, A. del Campo, J. Bill and F. Aldinger, Chem. Mater., 18, 2016–2020 (2006).
[4] K. Govender, D.S. Boyle, P.B. Kenway and P. O'Brien, J. Mater. Chem., 14, 2575–2591 (2004).
[5] K. Kakiuchi, E. Hosono and S. Fujihara, J. Photochem. Photobiol. A: Chem., 179, 81–86 (2006).
[6] S. Ueno and S. Fujihara, J. Electrochem. Soc., 158, K1–K5 (2011).
[7] E. Hosono, T. Tokunaga, S. Ueno, Y. Oaki, H. Imai, H. Zhou and S. Fujihara, J. Ceram. Soc. Jpn., 120, 171–174 (2012).
[8] K. Kakiuchi, M. Saito and S. Fujihara, Thin Solid Films, 516, 2026–2030 (2008).
[9] S. Inoue and S. Fujihara, Langmuir, 26, 15938–15944 (2010).
[10] W. Stählin and H.R. Oswald, Acta Cryst., B26, 860–863 (1970).
[11] S.P. Newman and W. Jones, J. Solid State Chem., 148, 26–40 (1999).
[12] Q. Hou, L. Zhu, H. Chen, H. Liu and W. Li, Electrochim. Acta, 78, 55–64 (2012).
[13] W. Sun, K. Wu, M.A. Thomas, F. Meng, X. Song, Z. Sun, Z. Zhang and J. Cui, J. Electrochem. Soc., 160, D558–D564 (2013).
[14] Y.H. Lai, C.Y. Lin, H.W. Chen, J.G. Chen, C.W. Kung, R. Vittal and K.C. Ho, J. Mater. Chem., 20, 9379–9385 (2010).
[15] Y. Qiu, W. Chen and S. Yang, J. Mater. Chem., 20, 1001–1006 (2010).
[16] H. Utsunomiya, S. Ueno and S. Fujihara, Key Eng. Mater., 582, 206–209 (2014).
[17] L. Poul, N. Jouini and F. Fiévet, Chem. Mater., 12, 3123–3132 (2000).
[18] E. Hosono, S. Fujihara, T. Kimura and H. Imai, J. Colloid Interface Sci., 272, 391–398 (2004).
[19] X. Hu, X. Shen, R. Huang, Y. Masuda, T. Ohji and K. Kato, J. Alloys Compd., 580, 373–376 (2013).
[20] S. Yamabi and H. Imai, J. Mater. Chem., 12, 3773–3778 (2002).
[21] S. Ueno and S. Fujihara, Key Eng. Mater., 445, 117–120 (2010).
[22] M.K. Nazeeruddin, Z. Kay, I. Rodicio, R. Humphry-Baker, E. Müller, P. Liska, N. Vlachopoulos and M. Grätzel, J. Am. Chem. Soc., 115, 6382–6390 (1993).
[23] M. Grätzel, Inorg. Chem., 44, 6841–6851 (2005).
[24] T. Biswicka, W. Jonesa, A. Pacułab, E. Serwickab and J. Podobinski, J. Solid State Chem., 180, 1171–1179 (2007).
[25] W. Stählin and H.R. Oswald, J. Solid State Chem., 3, 252–255 (1971).
[26] J.P. Auffredic and D. Louër, J. Solid State Chem., 46, 245–252 (1983).
[27] S. Ueno, H. Utsunomiya and S. Fujihara, Key Eng. Mater., 582, 202–205 (2014).